Experimental section

1. Synthesis of Sn-doped hematite nanowires

Hematite (α-Fe_2O_3) nanowires were prepared on a fluorine-doped tin oxide (FTO) glass substrate by a previously reported method.[1] A Teflon-lined stainless steel autoclave was filled with 20 ml aqueous solution containing 0.15 M of ferric chloride ($FeCl_3 \cdot 6H_2O$, Acros, 99+%) and 1 M sodium nitrate ($NaNO_3$, Fisher 99.4%). The solution pH was adjusted to 1.5 by HCl. A pre-cleaned piece of FTO glass substrate was put into the autoclave. The autoclave was heated at 95 °C for 4 hrs and allowed to cool down at ambient conditions. A uniform layer of iron oxyhydroxide (α-FeOOH) film (yellow in color) was formed on the FTO substrate. The α-FeOOH film was washed with deionized (DI) water to remove residual salt. To introduce Sn-doping into the nanowires, we intentionally added 1-2 drops of tin (IV) chloride ($SnCl_4$) ethanol solution (2 mg/ml) onto the α-FeOOH film, and then sintered in air at 550 °C for 30 min, followed by annealing at 800 °C for additional 20 min.[2]

2. Acid treatment

Hematite nanowires grown on FTO glass substrate were immersed in pure acetic acid (99.8%) for 5 min, and then let them dry in air without washing. Then the acid-treated hematite nanowires were further annealed at 450 ^{o}C in air for 30 min. Hematite nanowire films were treated with other inorganic acids (2 M HCl, 2 M HNO_3, 1 M H_3PO_4) using the same procedure.

3. Dye adsorption and desorption measurements

Untreated hematite nanowire film and acid treated hematite nanowire film with geometric area of 0.5 cm^2 was immersed into a 30 mg/L methylene blue aqueous solution for 24 hrs. Then the sample was gently rinsed with DI water and air dried. Each dried sample was immersed into acetonitrile for 15 min to allow desorption of dye molecules. The absorbance of solutions containing desorbed dye molecules were measured with the UV–vis spectrometer (U-3000, Hitachi High-Technologies Corporation). The characteristic absorbance peak at 655 nm is a good indicator of the amount of desorbed dye molecules, and thus, the surface area of hematite sample.

4. Material characterization

Scanning electron microscopy (SEM) images were collected with a field-emission SEM (Hitachi S-4800 II). X-ray diffraction (XRD) spectra were collected with a Rigaku Americas Miniflex Plus powder diffractometer. Diffraction spectra were recorded from a 2θ angle of 20 to 80 degree with a step size of 0.04 degree at a rate of 1 degree/min. X-ray Photoelectron Spectroscopy (XPS) was performed on a RBD upgraded PHI-5000C ESCA system (Perkin-Elmer) using Al-monochromatic X-ray at a power of 25 W with an X-ray-beam diameter of 10 mm, and a pass energy of 29.35 eV. The pressure of analyzer chamber was maintained below 5×10^{-8} Pa during the measurement. The binding energy was calibrated using the C 1s photoelectron peak at 284.6 eV as the reference.

5. Photoelectrochemical and electrochemical measurements

Hematite nanowires were fabricated into photoanodes by soldering a copper wire onto a bare part of the FTO substrate. The substrate edges and the metal contact region were sealed with insulating epoxy resin. The working electrode area is in the range of 0.2-0.25 cm^2. 1 M NaOH aqueous solution (pH = 13.6) was used as electrolyte for hematite electrodes. Linear sweeps, *I-t* curves and electrochemical impedance spectra were collected by a CHI 660D electrochemical station, with Pt sheet as counter electrode and Ag/AgCl as reference, under simulated sunlight (100 mW/cm^2) generated from a 150 W xenon lamp (Newport 6255) coupled with an AM 1.5 global filter (Newport 81094). Incident-photon-to-current-conversion-efficiency (IPCE) data were collected by the CHI 660D electrochemical station with a solar simulator (Newport 69920, 1000 W xenon lamp), coupled with an infrared water filter (Oriel 6127) and aligned monochrometor (Oriel Cornerstone 130 1/8 m). Charge separation efficiency is measured the photocurrent densities under 370 nm light illumination in 1 M NaOH solution with H_2O_2, according to the following equation [3]:

$$\text{Charge separation efficiency} = \frac{1240 J_{H_2O_2}}{P(\lambda)\times \lambda \times Abs(\lambda)}$$

Where λ is the incident wavelength, which is 370 nm, J_{H2O2} is the photocurrent density in 0.5 M H_2O_2 aqueous solution, P(λ) is the power density of irradiance at 370 nm, Abs (λ) is the amount of absorption at 370 nm.

Electrochemical impedance spectroscopy (EIS) was carried out by using the same electrochemical setup as PEC measurement. It was conducted in a range from 0.1 Hz to 100kHz at open circuit potential with a perturbation of 5 mV. ZSimpWin software was used to fit EIS data and obtain parameters of equivalent circuit elements. Mott-Schottky data was collected at 10kHz under the same condition as *I-V* dark scan. Donor density (N_d) can be estimated according to the Mott–Schottky equation:

$$N_d = (\frac{2}{e\varepsilon\varepsilon_0})[\frac{d(\frac{1}{C^2})}{dV}]^{-1}$$

Where e is the electron charge, ε is the dielectric constant of hematite (80), ε_0 is the permittivity of vacuum, and C is the capacitance derived obtained at each potential from the electrochemical impedance with 10 kHz frequency in the dark.

6. Transient measurements

The TA apparatus has been described elsewhere. [4] Briefly, the third harmonic of a Nd:YAG laser (Continuum, Surelite I-10, 355 nm, 4-6 ns pulse width) operating at 0.33 Hz is the UV excitation source. The repetition rate of the laser was chosen to ensure that all photogenerated charge carriers had fully decayed prior to the next excitation event. A laser intensity of ca.200 μJ cm^{-2} at 355 nm was incident on the photoelectrochemical cell, leading to an intensity of ca.100 μJ cm^{-2} at the sample. We note that high pump laser intensities can lead to excessively high electron-hole recombination rates and in mind of this we use the relatively low excitation power of ca.100 μJ cm^{-2} throughout, in order to limit/eliminate this effect. There are a number of past studies on hematite regarding these laser intensities which give us confidence that the parameters used here are relevant in providing useful information. [5] A 75 W Xe lamp (OBB Corp.) coupled to monochromator (OBB Corp., set to 4 nm resolution) acts as the probe light and the change in optical density of the sample is calculated by measuring the transmitted light using a Si Photodiode (Hamamatsu) and a homemade amplification system coupled to both an oscilloscope (Textronix TDS 220) and data acquisition card (National

Instruments NI-6221). In order to generate the TA spectra at a range of biases, 200 laser shots per wavelength were recorded. Accurate kinetic traces were recorded in a separate experiment using a minimum of 500 shots per wavelength. All TA experiments were carried out in PEC cell in degassed 1 M NaOH solutions under potentiostatic control at the potential indicated in the text. Transient photocurrent measurements were recorded using the same apparatus with the light from the Xe probe lamp blocked. The current was obtained by measuring the voltage drop across a 47 ohm resistor in series with the working and counter electrode.

7. Equations for kinetic model of the trapped electrons (Fig 4):

In this simplified model the trapped electrons can decay by two competing pathways. It follows that both the rate of total charge extraction and the recovery of the 575 nm bleach should have a common rate constant ($k_{tot} = k_{ext} + k_{rec}$) and the relative yield of extracted charge and recombination will depend on the relative rates of each step. In figure S11 we show that the rate of hole decay does not appear to be strongly affected by the acid treatment, indicating that k_{rec} remains largely unchanged and that the increased charge extraction yield is due to a change in k_{ext}

$$-\frac{\mathrm{d}[e^-_{trap}]}{\mathrm{dt}} = (k_{ext} + k_{rec})[e^-_{trap}] \quad \text{Eq. 1}$$

$$[e^-_{trap}]_t = [e^-_{trap}]_0 e^{-(k_{ext} + k_{rec})t} = \Delta\mathrm{OD}_{575\ nm} \quad \text{Eq. 2}$$

$$Photocurrent\ (Cs^{-1}) = \frac{\mathrm{d}[e^-_{ext}]}{\mathrm{dt}} = k_{ext}[e^-_{trap}]_t \quad \text{Eq. 3}$$

$$charge\ extracted = [e^-_{ext}]_t = [e^-_{trap}]_0 \frac{k_{ext}}{k_{ext} + k_{rec}} \left(1 - e^{-(k_{ext} + k_{rec})t}\right) \quad \text{Eq. 4}$$

$$charge\ extraction\ yield = [e^-_{trap}]_0 \frac{k_{ext}}{k_{ext} + k_{rec}} \quad \text{Eq. 5}$$

$$recombination = [e^-_{rec}]_t = [e^-_{trap}]_0 \frac{k_{rec}}{k_{ext} + k_{rec}} \left(1 - e^{-(k_{ext} + k_{rec})t}\right) \quad \text{Eq. 6}$$

$$recombination\ yield = [e^-_{trap}]_0 \frac{k_{rec}}{k_{ext} + k_{rec}} \quad \text{Eq. 7}$$

Supplementary Figures

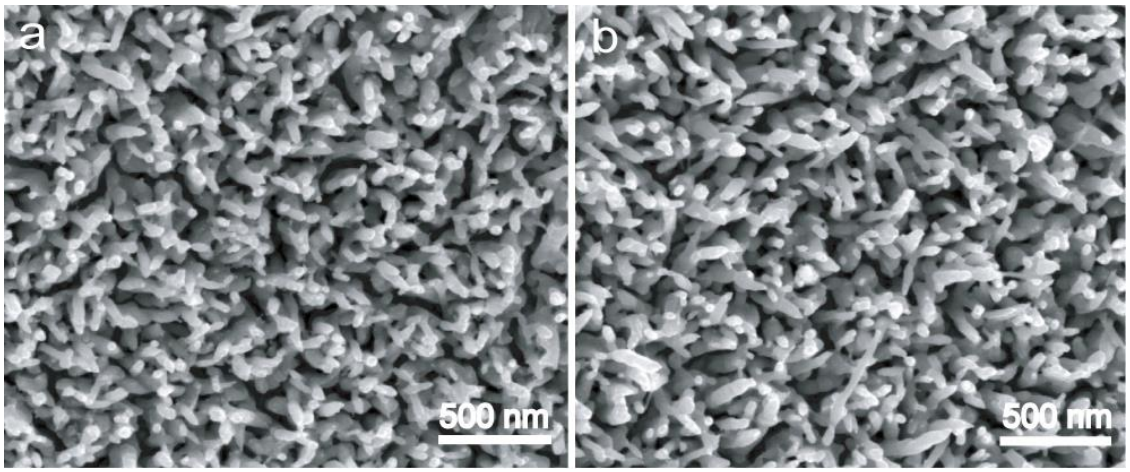

Fig S1. SEM images of (a) untreated hematite nanowires; and (b) acid-treated hematite nanowires.

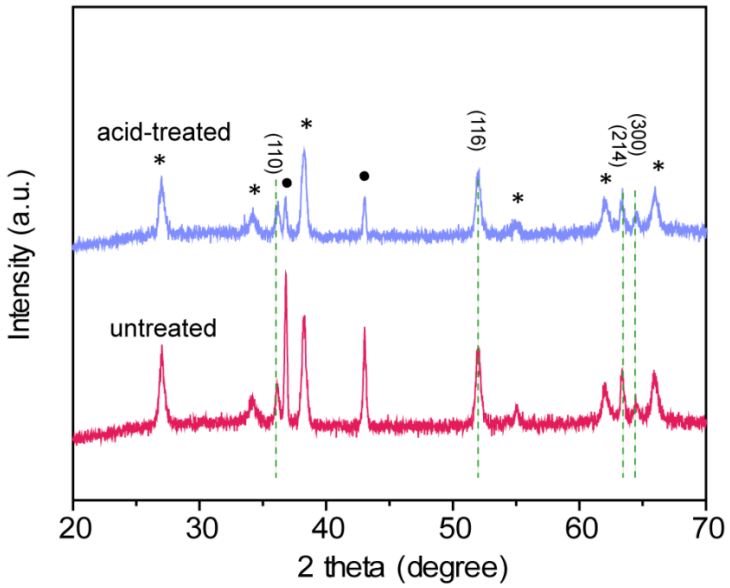

Fig S2. XRD spectra collected for untreated hematite and acid-treated hematite sample. Dashed lines highlight the characteristic diffraction peaks of hematite (JCPDS 33-0664). The asterisks and circles highlight the diffraction peaks of SnO_2 (JCPDS 41-1445) originated from FTO substrate and the peaks from aluminum substrate, respectively.

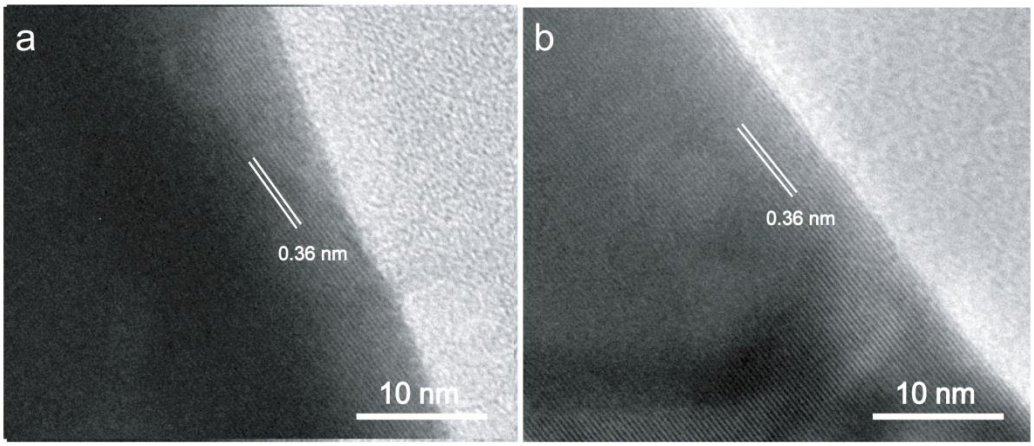

Fig S3. Lattice-resolved TEM images collected at the edge of (a) untreated hematite nanowire and (b) acid-treated hematite nanowire.

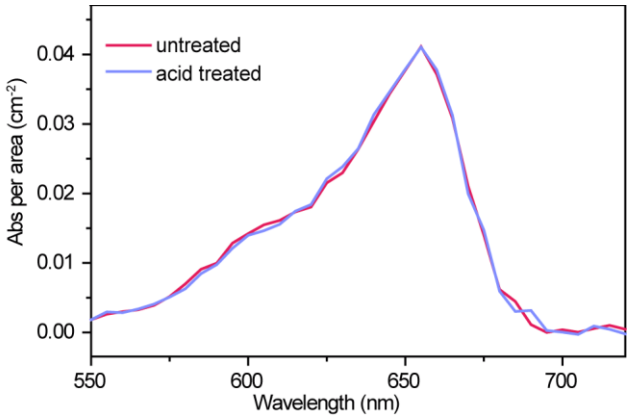

Fig S4. UV-Vis spectra collected for solutions containing methylene blue dye molecules desorbed from untreated hematite and acid treated hematite.

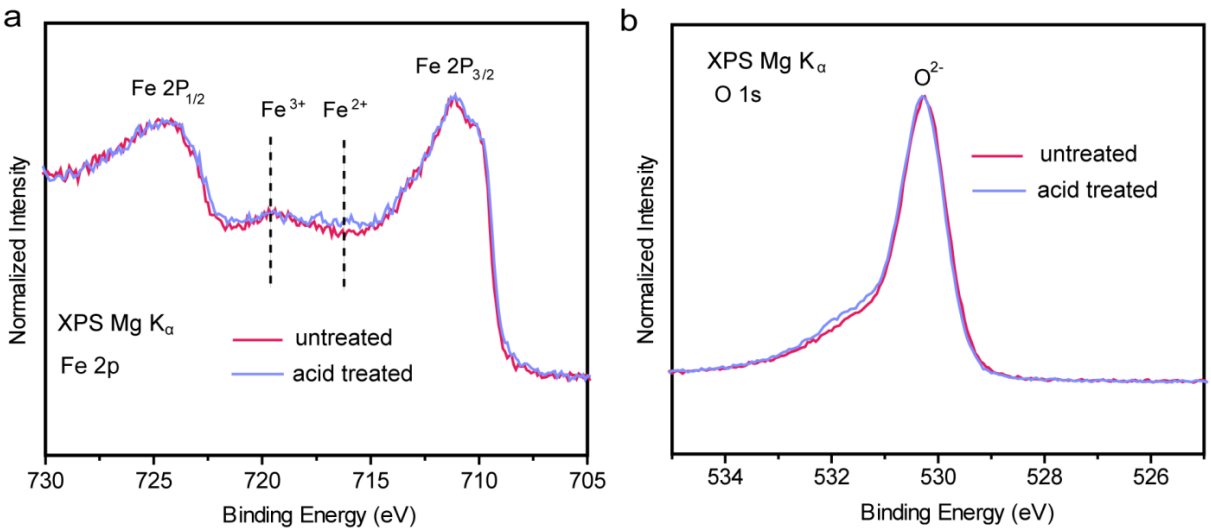

Fig S5. Overlay of normalized (a) Fe 2p and (b) O 1s XPS spectra of untreated hematite and acid-treated hematite samples. The dashed lines in (a) highlight the satellite peaks of Fe^{3+} and Fe^{2+} species.

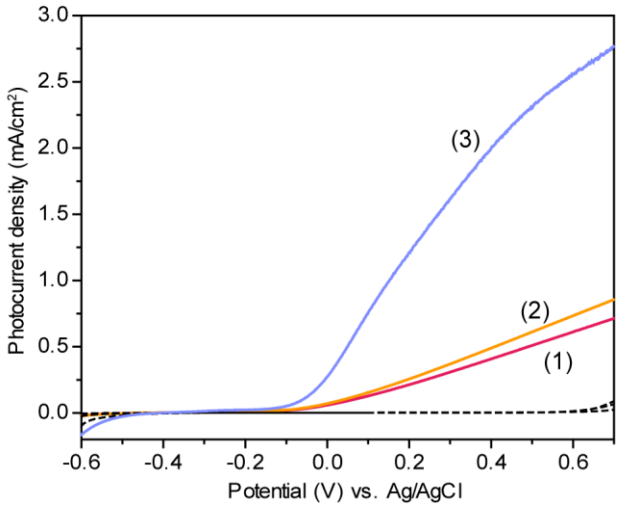

Fig S6. (a) Linear sweep voltammograms of (1) untreated hematite, (2) thermal annealed without acid treated hematite and (3) acid-treated hematite photoanodes recorded at 20 mV/s in a 1 M NaOH solution under illumination by simulated solar light of 100 mW/cm^2 and in the dark (dashed lines).

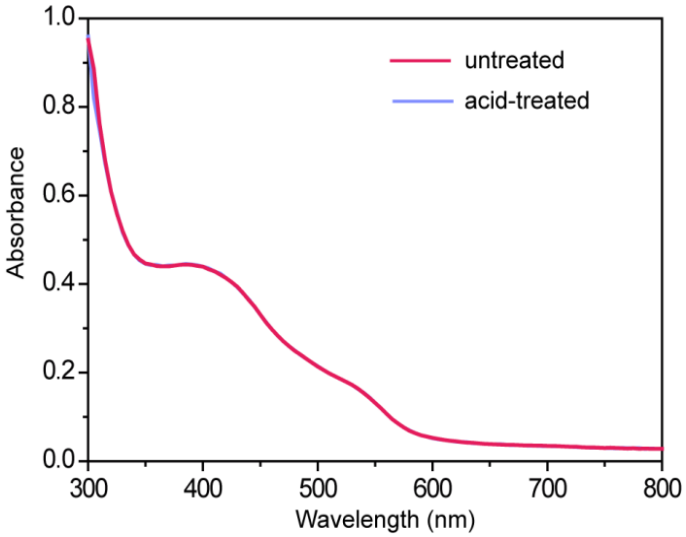

Fig S7. UV-vis spectra collected from untreated and acid-treated hematite sample.

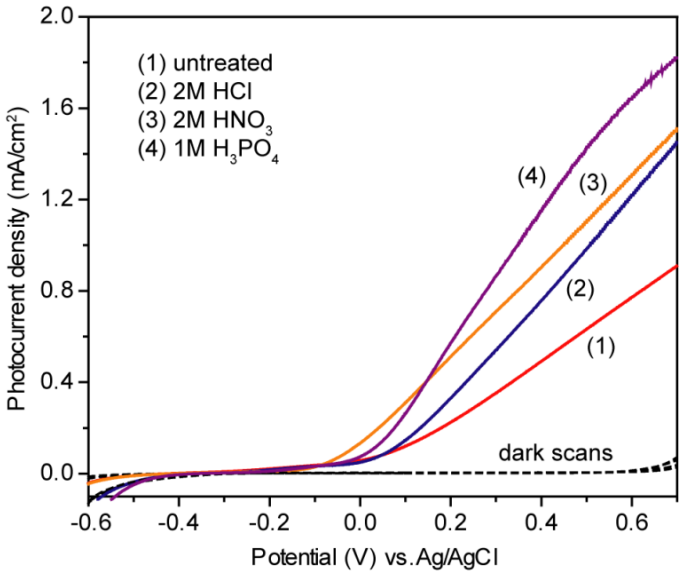

Fig S8. Linear sweep voltammograms collected for untreated hematite and hematite treated with different acids at 20 mV/s in a 1 M NaOH solution under illumination by simulated solar light of 100 mW/cm^2 and in the dark (dashed lines).

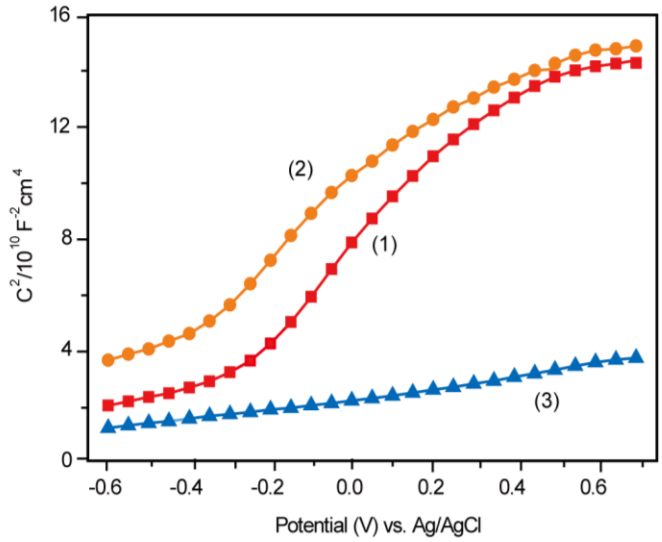

Fig S9. Mott-Schottky plots of (1) untreated hematite, (2) thermally annealed hematite without acid treatment and (3) acid treated hematite electrodes collected at 10 kHz in 1 M NaOH electrolyte in the dark.

Table S1. Parameters of equivalent circuit elements

Sample	R_s/Ù	R_{kt}/Ù	R_{ct}/Ù	Z_w/Ù•s$^{-0.5}$	C_d/F	C_t/F
Untreated Hematite	52.6	863.4	113.6	6.5e-6	1.4e-9	7.2e-7
Acid-treated hematite	19.3	238.7	5.1	2.4e-6	4.9e-9	8.1e-6

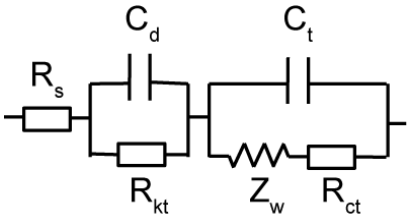

The equivalent circuit used to fit the EIS data: R_s is the series resistance, which includes the sheet resistance of the FTO substrate and the external contact resistance of the cell. The parallel elements, R_{kt}, C_d, R_{ct} and C_t, characterize the charge transfer resistance and the double layer capacitance for the hematite electrode and Pt counter electrode.

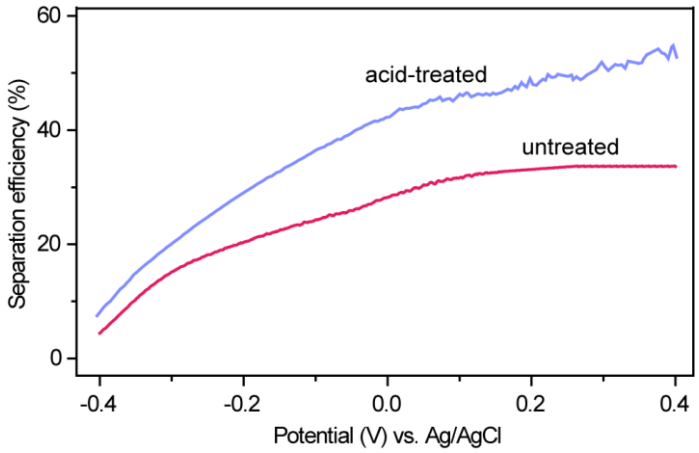

Fig S10. Plot of yield of charge separation against applied potential for untreated and acid-treated hematite photoanodes.

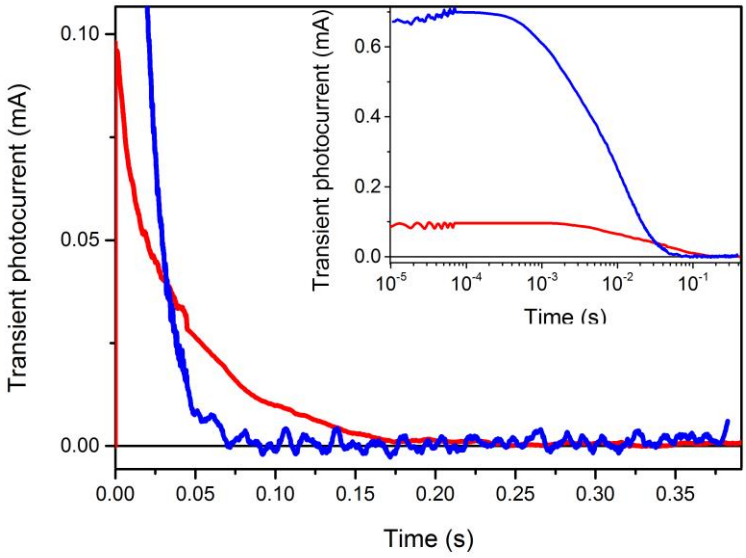

Fig S11. Transient photocurrent response of the acid treated (blue) and un-treated (red) Sn-Fe_2O_3 samples following UV laser (6 ns pulse, 355 nm, 100 μJ cm^{-2}, 0.33 H_z) excitation. The inset shows the same data plotted on a logarithmic scale.

TPC measurements also offer insights into the potential role of back electron transfer within a hematite electrode. Durrant *et al.* [6] have previously reported slow back electron transfer from the external circuit into the photoelectrode to be a efficiency limiting factor in a number of iron oxide materials, with such

transfer leading to electron-hole recombination. Back electron transfer can be identified by negative currents on the slow ms timescales in TPC caused by recombination between electrons in the bulk hematite and surface trapped holes. Notably in this instance, at the potentials studied (>0.2 V) there is no evidence for back electron transfer in either untreated or acid treated hematite suggesting that in these Sn-doped materials a significantly large electric field is present at 0.2 V Ag/AgCl to prevent electrons from reaching the surface trapped holes at the semiconductor-liquid junctions.

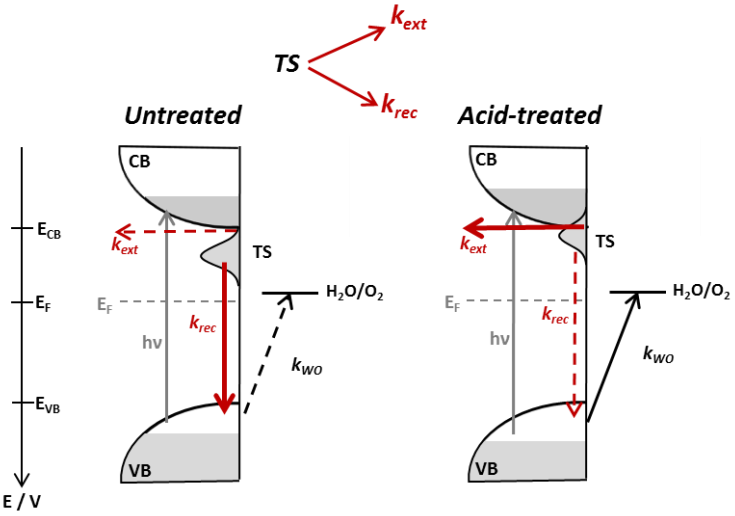

Fig S12. Proposed kinetic scheme of the untreated and acid-treated hematite electrodes held at 0.2 V following UV excitation (355 nm). The combined TA and TPC study indicates that electrons in the trap-state (TS), monitored at 575 nm using TA spectroscopy, can either recombine with surface trapped holes (k_{rec}) or be extracted to the external circuit (k_{ext}) as indicated by the red arrows (solid line being the dominant pathway). The acid treatment leads to a decrease in the recombination yield which is proposed to be due to an enhancement in the rate constant for k_{ext}, Fig S12.

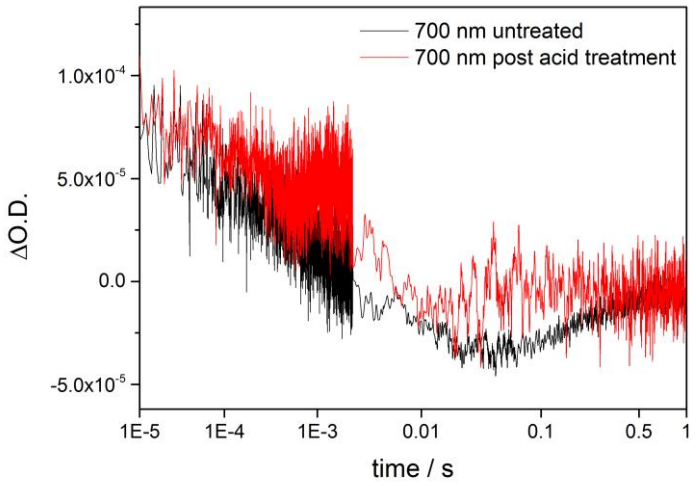

Fig S13. TA decays recorded at 700 nm for untreated and acid treated hematite under the same working conditions at 0.2 V vs. Ag/AgCl) following UV (355 nm, 6 ns pulse, 0.33 H_z, 100 μJ cm^{-2}) excitation of samples in 1 M NaOH. In figure S11 we show that the rate of hole decay does not appear to be strongly affected by the acid treatment, indicating that k_{rec} remains largely unchanged and that the increased charge extraction yield is due to a change in k_{ext}.

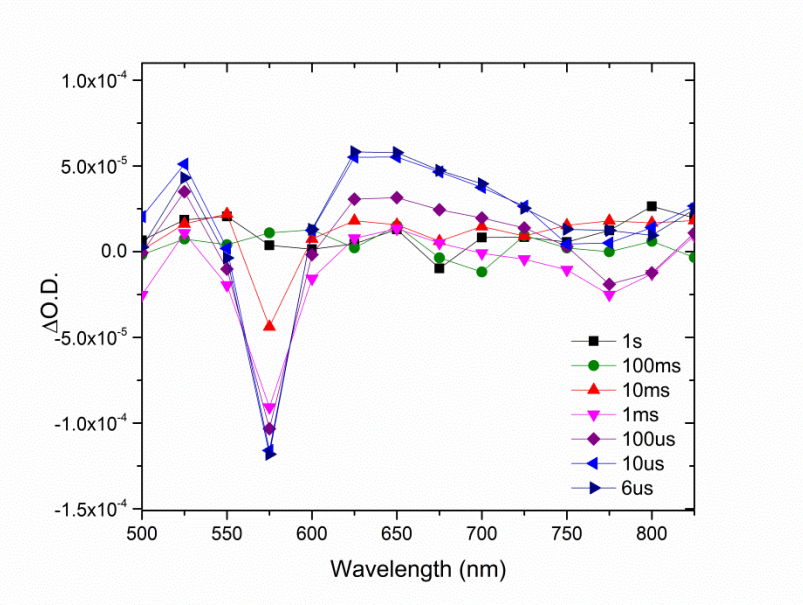

Fig S14. TA spectra under working photoelectrochemical conditions at an applied voltage of 0.2 V vs. Ag/AgCl for an untreated hematite that is thermally annealed in air at 450 ^{o}C for 30 minutes.

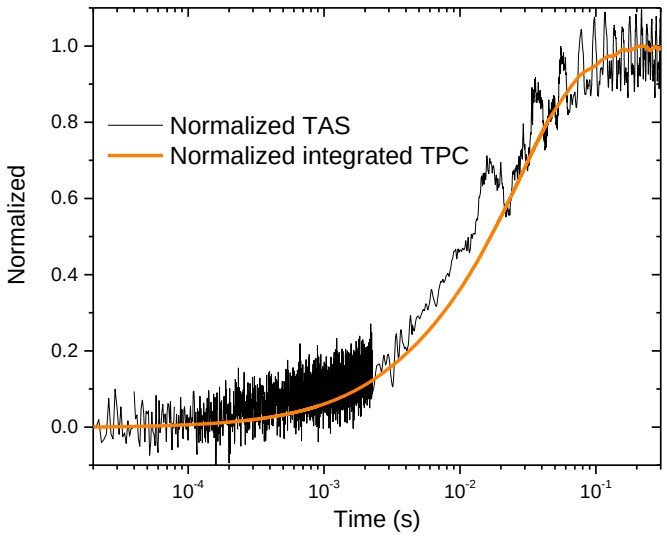

Fig S15. Overlay of 575 nm TA signal assigned to photoelectron trapping with the total charge passed derived from TPC under the same working conditions at 0.2 V vs. Ag/AgCl for an untreated hematite electrode that has been annealed in air at 450 ^{o}C for 30 minutes. Both curves are well fitted to single exponential decay functions yielding time constants of 21 ± 2 ms for the TAS and 25 ± 2 ms for the integrated TPC. The slightly increased rate of recovery of the 575 nm bleach following the thermal treatment is in-line with the very small improvement in photoelectrochemical activity upon thermal annealing. In contrast following acid treatment and thermal annealing the 575 nm feature recovers with a time constant of 7.1 ± 1 ms (main text)

Supporting references

[1] L. Vayssieres, N. Beermann, S. E. Lindquist, A. Hagfeldt, *Chem. Mater.* **2001**, *13*, 233-235.
[2] Y. C. Ling, G. M. Wang, D. A. Wheeler, J. Z. Zhang, Y. Li, *Nano. Lett.* **2011**, *11*, 2119-2125.
[3] H. Dotan, K. Sivula, M. Gratzel, A. Rothschild, S. C. Warren, *Energy Environ.Sci.* **2011**, *4*, 958-964.
[4] A. J. Cowan, J. W. Tang, W. H. Leng, J. R. Durrant, D. R. Klug, *J. Phys. Chem. C* **2010**, *114*, 4208-4214.
[5] S. R. Pendlebury, A. J. Cowan, M. Barroso, K. Sivula, J. H. Ye, M. Gratzel, D. R. Klug, J. W. Tang, J. R. Durrant, *Energy Environ.Sci.* **2012**, *5*, 6304-6312.
[6] S. R Pendlebury, X. Wang, F. Le Forma, M. Cornuz, A. Kafizas, S. D. Tilley, M.Grätze, J. R. Durrant, *J. Am. Chem. Soc.* **2014**, *136*, 9854–9857.